Section 3

Computational studies including new techniques, parallel processing, GPUs. Effects of model resolution.

Numerical Simulation of Heavy Rainfall Event Associated with Typhoon Hagibis (2019) with Different Horizontal Resolutions

Kentaro Araki[1]

1: Meteorological Research Institute, Tsukuba, Ibaraki, Japan

e-mail: araki@mri-jma.go.jp

1. Introduction

Heavy rainfall event occurred in eastern and northern areas in Japan on 11-13 October 2019 during the passage of the typhoon Hagibis (2019), and more than 100 people were killed or missing as a result of the devastating floods and landslides (according to a report by the Fire and Disaster Management Agency of Japan on February 12, 2020). The operational mesoscale model of the Japan Meteorological Agency (JMA) successfully forecasted the occurrence of the heavy rainfall events, but a quantitative forecast of precipitation amount remains challenges. During this heavy rainfall event, precipitation was enhanced especially in the mountain areas, and the maximum precipitation amount during the event exceeded 1,000 mm (Fig. 1). In this study, in order to investigate the quantitative predictability of the heavy rainfall, we performed a case study on this events through the analysis of observation data and numerical simulations, and examined the environmental conditions, important factors, and numerical model representation for heavy rainfall.

2. Model settings

Numerical simulations were performed by the JMA Non-Hydrostatic Model (NHM) with a domain of 2,500 x 2,500 km covering Japan and horizontal resolutions of 5 km (5km-CNTL), 2 km (2km-CNTL), and 1 km (1km-CNTL). A convection parameterization scheme was not used in these experiments, but an additional experiment using the Kain-Fritsch scheme was performed for the horizontal resolution of 5 km. A bulk cloud microphysics scheme with 2-moment cloud water, cloud ice, snow, and graupel was used and the Mellor-Yamada-Nakanishi-Niino scheme was applied for the turbulence closure scheme in all experiments. The initial and boundary conditions were provided from the 3-hourly JMA mesoscale analysis data and the models were run from 09 JST (JST=UTC+9h) on 11 to 15 JST on 13 October 2019. Other setups were the same as those used by Saito et al. (2006). In order to investigate the effect of orography, we also performed experiments in which the mountains of Honshu were removed and the elevation was set to 0 m (5km-, 5km-KF, 2km-, and 1km-NOZS), and experiments in which the land was removed for each horizontal resolution (5km-, 5km-KF, 2km-, and 1km-NOLN).

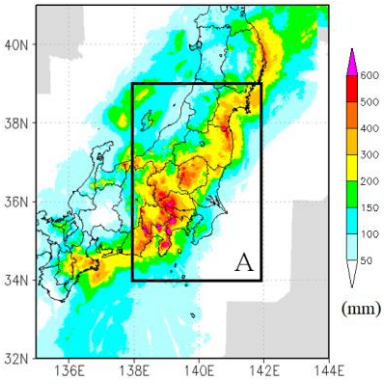

Figure 1. Precipitation amount from 09 JST on 11 to 12 UTC on 13 October 2019 derived from Radar analysis (RA).

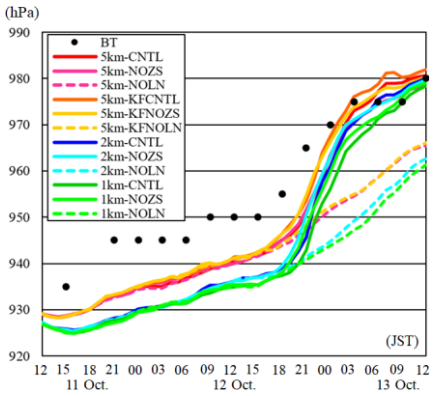

Figure 2. Time series of RMSC Tokyo best track (BT) central pressure and simulated central pressures.

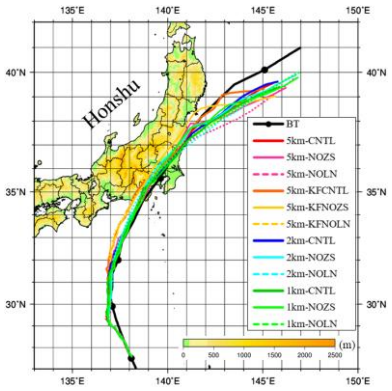

Figure 3. RMSC Tokyo BT and simulated tracks from 09 JST on 11 to 12 JST on 13.

3. Representations of typhoon Hagibis (2019) and precipitation amount

The typhoon moved northward to the south of Japan on 11 October and made landfall around 19 JST on 12 October. Precipitation intensified on the north side of the center of the typhoon, and heavy rainfall had started before the typhoon made landfall. The case study using the analysis data and observation data indicated that the important factors of heavy rainfall were the large supply of water vapor, the formation and intensification of a front on the north side of the typhoon during the transformation of the typhoon into an extratropical cyclone, the enhancement of precipitation by orography, and the direct influence of developed convective clouds near the center of the typhoon (not shown).

Time series of the Regional Specialized Meteorological Center (RSMC) Tokyo best track (BT) central pressure and simulated central pressures are shown in Fig. 2. The central pressures were smaller than the best track in each experiment, but the temporal variations were reproduced successfully. In NOLN experiments, the rise in central pressure after 18 JST on 12 was slower than in others because of the lack of weakening of the typhoon at the time of landfall. The paths of the typhoon were almost the same as the best track in each experiment (Fig. 3). In the experiments using the KF scheme, the central pressures were higher than in the others and the paths were slightly northward.

Figure 4 shows horizontal distributions of precipitation amount simulated by each experiment, and a summary of central pressures, delays of typhoon movement, and precipitation amounts in the domain A (rectangle in Figs. 1 and 3) is given in table 1. Compared with the radar analysis (RA), the distribution of heavy rainfall areas was reproduced in all

CNTL experiments, and the precipitation amount averaged in the domain A was well reproduced in all CNTL experiments except for 5km-KFCNTL. On the other hand, the maximum precipitation amounts reached more than 1000 mm for the 2km-CNTL only, and were underestimated for the other CNTL experiments. In NOZS experiments, precipitation amounts were reduced compared to the CNTLs at all horizontal resolutions, but the heavy rainfall itself was reproduced. It is indicated that the heavy rainfall was caused by the front that formed and intensified on the north side of the typhoon. In the CNTL experiments, precipitation enhancement through the Seeder-Feeder mechanism occurred due to rainfall on the low-level feeder clouds formed by the orographic updraft on the windward slopes of the mountains; this precipitation enhancement did not occur in the NOZS experiments and the contributions of orographic precipitation to the total precipitation amounts in the CNTL experiments ranged from 75-85% at each horizontal resolution. In the NOLN experiments, the area of heavy rainfall were shifted to the north of those in the CNTLs and NOZSs, and the maximum precipitation amounts in the domain A were smaller than in NOZSs for each resolution.

In this study, the experiment with a horizontal resolution of 2 km showed the best reproducibility of heavy rainfall associated with Hagibis (2019). The results of this study indicate that the large water vapor supply and the front formed and intensified in the north of the typhoon were important factors of the heavy rainfall, and that precipitation was significantly enhanced by the orographic effect through the Seeder-Feeder mechanism. The underprediction of the maximum precipitation amount at 1km-CNTL might be due to the failure to reproduce the structures of the typhoon and the front.

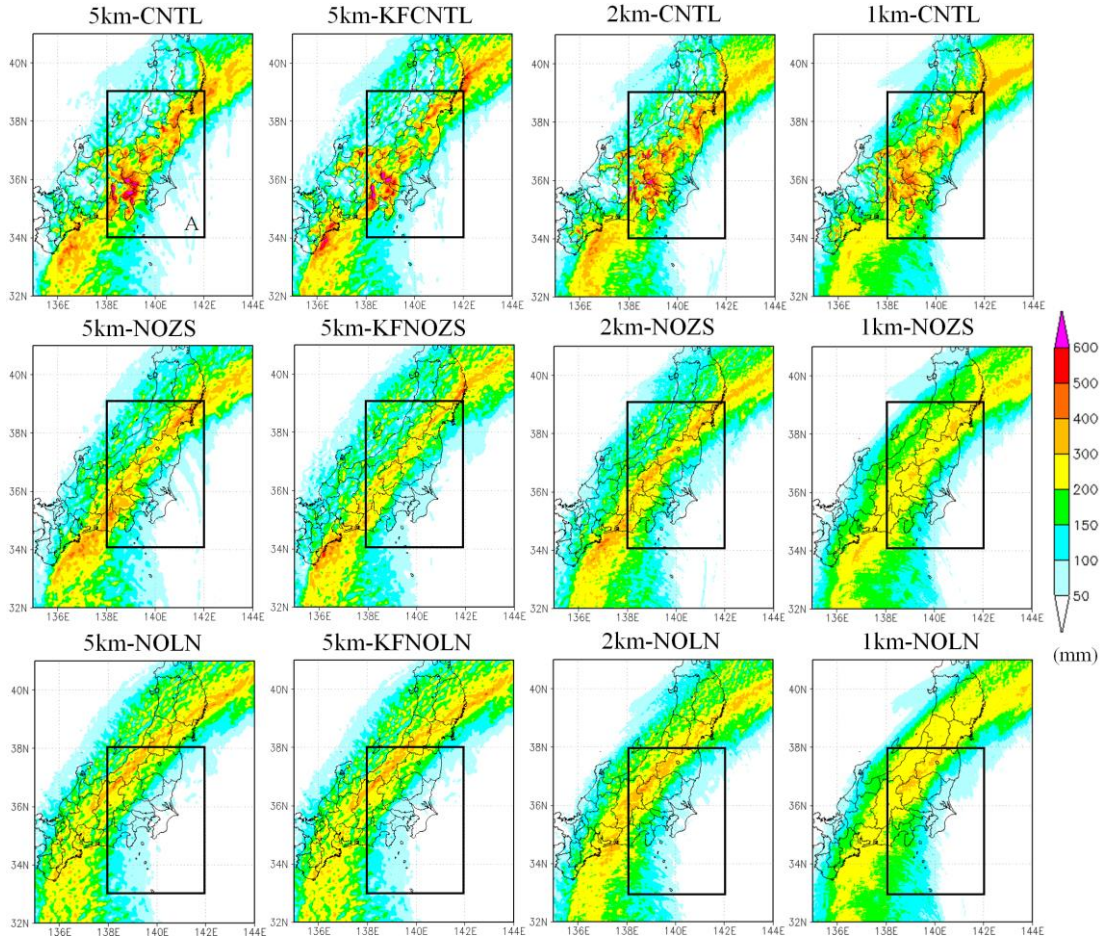

Figure 4. Horizontal distribution of precipitation amounts from 09 JST on 11 to 12 JST on 13 October 2019 in each experiment.

Table 1. Summary of central pressures at the longitude of 138.7°E, delays of typhoon movement, and precipitation amounts in the domain A (rectangle in Figs. 1 and 4). The values under the precipitation amounts from 09 JST on 11 to 12 JST on 13 October of each sensitivity experiment indicate the decrease rate (%) from the precipitation amount of CNTL.

	BT / RA	5km-CNTL	5km-NOZS	5km-NOLN	5km-KFCNTL	5km-KFNOZS	5km-KFNOLN	2km-CNTL	2km-NOZS	2km-NOLN	1km-CNTL	1km-NOZS	1km-NOLN
Central pressure at longitude of 138.7°E (hPa)	955	949.6	946.5	946.0	961.4	953.0	945.9	945.1	941.6	940.0	942.5	938.8	939.1
Delay of typhoon movement (hour)	(18 JST on 12)	2	0	1	4	2	3	2	0	1	2	0	1
Averaged precipitation amount in domain A (mm)	163.8	161.3	136.8	121.5	142.8	120.1	121.5	159.2	138.3	136.6	167.0	144.9	143.8
			15.2%	24.6%		15.9%	14.9%		13.1%	14.2%		13.2%	13.9%
Maximum precipitation amount in domain A (mm)	1346.1	788.5	520.1	519.2	766.8	454.2	519.2	1135.6	461.4	472.8	841.1	358.7	361.6
Averaged difference of precipitation amount in domain A (mm)	-	-	24.5	39.7	-	22.7	21.2	-	20.9	22.6	-	22.0	23.1
Maximum difference of precipitation amount in domain A (mm)	-	-	507.7	710.0	-	543.6	592.7	-	902.9	808.8	-	614.0	599.8
Averaged contribution rate of orographic precipitation in CNTL (%)	-	-	13.7	26.5	-	15.5	17.3	-	12.6	14.0	-	11.2	12.3
Maximum contribution rate of orographic precipitation in CNTL (%)	-	-	84.6	91.1	-	83.7	87.7	-	79.9	82.4	-	74.9	78.4

Computational Performance Improvements in GFSv16

Jun Wang[1*], Jeffrey Whitaker[2], Edward Hartnett[3, 7], James Abeles[4], Gerhard Theurich[5], Wen Meng[4], Cory Martin[6], Jose-Henrique Alves[8], Fanglin Yang[1], Arun Chawla[1]

[1]NOAA/NWS/NCEP/EMC, [2]NOAA/ESRL/PSD, [3]NOAA/ESRL/GSD. [4]IMSG@NOAA/NWS/NCEP/EMC, [5]ESMF/NRL/SAIC, [6]RedLine@NOAA/NWS/NCEP/EMC,[7]CIRES, University of Colorado,[8]SRG@NOAA/NWS/NCEP/EMC

[*]Jun.Wang@noaa.gov

Introduction:

NCEP is developing its next version of the medium-range weather Global Forecast System (GFSv16) for operational implementation in 2021. One major upgrade in GFSv16 is to raise the model top from 54km to 80km, while increasing the number of vertical levels from 64 to 127. This change, along with other new physics upgrades, significantly increases the computational cost and the output data amount. In this paper, we describe technical advances made to improve the GFSv16 computational performance.

Model description:

The prognostic model of GFSv16 is the Unified Forecast System (UFS) model with the atmosphere being one-way coupled with an ocean wave model through the NOAA Environmental Modeling System (NEMS) infrastructure. The NEMS is built upon the Earth System Modeling Framework (ESMF) and uses the National Unified Operational Prediction Capability (NUOPC) Layer. The atmosphere component consists of the Finite-Volume Cubed-Sphere Dynamical Core (FV3), GFS physics package and write grid components running at the C768L127 resolution. The wave component uses the NOAA WAVEWATCH III model (WW3) with a global grid mosaic [WW3DG, 2019]. WW3 global core resolution is increased from ½ degree to ⅙ degree. The model produces forecast history files in netcdf format and post-processed grib2 files out to 16 days, four times a day with hourly output for the first 120 hours and then three-hourly output up to 384 hours.

Technical improvements:

Four major technical improvements have been applied to GFSv16. They are described below.

1) Inline post on write grid component

In GFSv15, the asynchronous IO technology was applied to set up the write grid components running on groups of MPI tasks which are different from forecast MPI tasks. The write grid components receive data from forecast tasks through various regridding methods and then output history files, while the forecast tasks simultaneously conduct integration. In GFSv16, an inline post capability is added to reduce the IO activity in the whole computer system (Fig. 1). With the inline post implementation, the total time needed to generate a 2.5GB GRIB2 GFS master file at a single forecast time is reduced from 211s in a standalone post to 39s when both are run with 84 tasks on the NCEP WCOSS operational computer.

2) Parallel writing compressed netcdf history files

Due to the atmosphere component vertical resolution increase, forecast output data is doubled, and the time to read and write these data also increases significantly. In GFSv16 the history file data format is switched from the previous plain binary NEMSIO format to netCDF/HDF5 format, with bit-smoothing, zlib compression and the data quantizing method described in [Silver & Zender, 2017]; the size of a single 3D fields history file is reduced from 33.6GB to 6.3GB with acceptable precision loss. Through the collaboration between EMC and the NetCDF working group, Unidata released a new NetCDF version with the capability of writing compressed data in parallel. The corresponding interface is implemented in GFSv16. This new feature enables

GFSv16 to write out a single lossy compressed 3D history file in 43s, a reduction from 441s without parallelization. The new method also makes it possible to reduce the overall model computing cost.

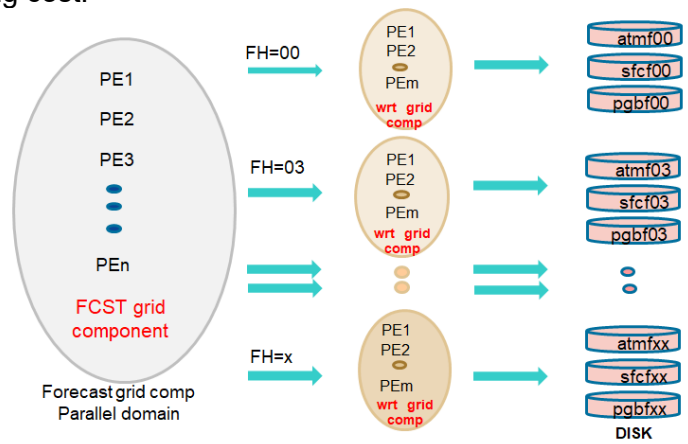

Fig 1. Parallelization of GFSv16 write grid component with inline post.

3) Scalability improvement in WW3

A scalability issue was uncovered in WW3 in the GFSv16 experiments. A threading issue and improper field gather operation were identified and fixed in WW3. The fixes improved WW3 scalability. When tripling the number of MPI tasks, WW3 now takes about 36% of the original run time, while before these fixes it took about 94% of the original run time.

4) Data transfer improvement ESMF model components

While running GFSv16 experiments, a persistent delay was found on forecast tasks when they transfer data to the write tasks. The ESMF support group identified the underlying issue and fixed the problem by writing all the messages sent to the same destination write task into a buffer and then sending the whole message via a single MPI_Isend(). This fix allows each data transfer time on forecast tasks to be reduced from 4s to less than 0.5s. This method is also applied to the NUOPC connector that allows the atmosphere model to send data to the wave model.

Future work:

NCEP is quickly approaching exascale computing in the next few years when a fully coupled atmosphere, ocean, ice and wave system is developed and higher resolutions are chosen for the components. Future development to solve the challenges include: 1) developing computationally efficient components in the coupled system; 2) developing an efficient system integration strategy; 3) developing efficient IO with prudently chosen output fields, efficient compression algorithms and proper data representation; 4) reorganizing the workflow to reduce IO stress on the computer system; and 5) exploring other technologies such as cloud computing, GPU computing, etc.

References:

Silver, J. D. and Zender, C. S.: The compression–error trade-off for large gridded data sets, Geosci. Model Dev., 10, 413–423, https://doi.org/10.5194/gmd-10-413-2017, 2017

The WAVEWATCH III® Development Group (WW3DG), 2019: User manual and system documentation of WAVEWATCH III® version 6.07. Tech. Note 333, NOAA/NWS/NCEP/MMAB, College Park, MD, USA, 326 pp. + Appendices.